HIV-1 Capsid Protein Forms Spherical (Immature-Like) and Tubular (Mature-Like) Particles in Vitro: Structure Switching by pH-induced Conformational Changes

Lorna S. Ehrlich,* Tianbo Liu,† Suzanne Scarlata,‡ Benjamin Chu,† and Carol A. Carter*
Departments of *Molecular Genetics & Microbiology, †Chemistry, and ‡Physiology & Biophysics, State University of New York at Stony Brook, Stony Brook, New York 11794 USA

ABSTRACT The viral genome and replicative enzymes of the human immunodeficiency virus are encased in a shell consisting of assembled mature capsid protein (CA). The core shell is a stable, effective protective barrier, but is also poised for dissolution on cue to allow transmission of the viral genome into its new host. In this study, static light scattering (SLS) and dynamic light scattering (DLS) were used to examine the entire range of the CA protein response to an environmental cue (pH). The CA protein assembled tubular structures as previously reported but also was capable of assembling spheres, depending on the pH of the protein solution. The switch from formation of one to the other occurred within a very narrow physiological pH range (i.e., pH 7.0 to pH 6.8). Below this range, only dimers were detected. Above this range, the previously described tubular structures were detected. The ability of the CA protein to form a spherical structure that is detectable by DLS but not by electron microscopy indicates that some assemblages are inherently sensitive to perturbation. The dimers in equilibrium with these assemblages exhibited distinct conformations: Dimers in equilibrium with the spherical form exhibited a compact conformation. Dimers in equilibrium with the rod-like form had an extended conformation. Thus, the CA protein possesses the inherent ability to form metastable structures, the morphology of which is regulated by an environmentally-sensitive molecular switch. Such metastable structures may exist as transient intermediates during the assembly and/or disassembly of the virus core.

INTRODUCTION

The viral genome and replicative enzymes of the human immunodeficiency virus (HIV) are encased in a conical shell that is assembled from a single protein subunit, the capsid protein (CA, p24) (Gelderblom, 1991; Welker et al., 2000). The composite structure, referred to as the core, is formed during the late stage of virus assembly and serves to protect the viral genome as the mature infectious viral particle makes a temporary existence in an extracellular environment. When the virus particle eventually encounters a new host, virus entry commences. Fusion of the viral membrane with the host plasma membrane results in the opening of a small channel, connecting the interior of the viral particle with the host cytoplasmic compartment. Grewe et al. (1990) demonstrated that at this early stage the core becomes EM-invisible indicating loss of its characteristic conical morphology. Clearly, the core shell is a stable, effective protective barrier, but also is poised for dissolution on cue to allow transmission of the viral genome into its new host. That the CA protein is able to meet the opposing exigencies of assembly and disassembly implies a sensitivity and a responsiveness to appropriate environmental cues. We hypothesize that this ability is an inherent characteristic of the CA protein.

Received for publication 16 October 2000 and in final form 6 April 2001.
Address reprint requests to Dr. Carol Carter, SUNY Stony Brook, Department of Molecular Genetics and Microbiology, Life Science Building, RM 248, Stony Brook, NY 11794. Tel: 631-632-8801; Fax: 631-632-9797; E-mail ccarter@ms.cc.sunysb.edu.

0006-3495/01/07/586/09 $2.00

The response of mature CA protein to selected environmental cues were examined by us and others in in vitro assembly studies. We initially examined the self-assembly capabilities of purified recombinant mature HIV-1 CA protein and found that, with only pH and NaCl as assembly triggers, the protein formed large tubular or rod-like structures that were detected by negative staining electron microscopy (Ehrlich et al., 1992). Others (Gross et al., 1997, 2000; von Schwedler et al., 1998) have since confirmed the intrinsic ability of mature HIV-1 CA protein to form this structure. This has been the only form of in vitro assembled CA detected by negative staining or thin section EM in studies published to date giving the impression that the protein has limited conformational flexibility. However, this static response of the CA protein to several permutations of pH, salt, and divalent ions may not reflect the entire range of the CA protein ability because 1) only structures stable to the preparative procedures required for electron microscopy will be detected and 2) disassembly into small oligomers, which might occur under some conditions, would be missed because EM is not the appropriate technique for oligomer detection. This may be similar to the limitations encountered when examining the fate of the core during viral entry.

In the present study, we employed static light scattering (SLS) and dynamic light scattering (DLS) (Chu, 1991), instead of EM, to assess the conformational flexibility of the CA protein from the range of its response to changes in the pH of the protein solution. For monitoring pH-induced changes in the CA protein, SLS and DLS were chosen because both techniques are based on analysis of hydrodynamic properties and, as such, permit characterization of

proteins as they exist unperturbed in solution. The positive correlation between light scattering intensity and molecular size permits detection of large structures despite their low representation in a sample. DLS allows studies to be conducted under ionic strength conditions close to physiological levels that cannot be used for optimal EM studies (Gross et al., 1997). The combination of SLS and DLS can be very powerful in quantitatively characterizing particles, including biological macromolecules in solution, by obtaining the particle mass, size, size distribution, shape and inter-particle interactions. We chose pH as test environmental cue to allow us to relate our findings to HIV capsid disassembly during virus entry. HIV particles utilize both receptor-mediated and endocytic entry modes for internalization during natural infection (Grewe et al., 1990; Marechal et al., 1998; Fackler and Peterlin, 2000; Schaeffer et al., 2001). It is known that the low pH in the endocytic compartment (Marsh, 1984) serves as cue for functional capsid disassembly of several picorviruses (Phelps et al., 2000). It has yet to be determined whether this is also applies to HIV.

In this report, detection of a CA multimer with spherical morphology is documented for the first time. The switch from rod-like to spherical morphology occurred within a narrow physiological pH range (i.e., pH 7.0 to pH 6.8). Below this range, disassembly into dimers occurred. These observations suggest that the CA multimer has a metastable nature whose morphology and stability is regulated by a pH-sensitive molecular switch.

MATERIALS AND METHODS

Protein preparation

Recombinant HIV-1 CA protein was expressed in *Escherichia coli* from an expression plasmid encoding Gag-PR and purified to near-homogeneity using a non-denaturing protocol described previously (Ehrlich et al., 1990). Aliquots of purified CA proteins were placed in dialysis tubing (MW cutoff, 1 kDa) and dialyzed against 1000 volumes of 10 mM sodium phosphate buffer with the specified pH at 5°C for 12 to 24 h with several buffer changes. Dialyzed protein samples were diluted with buffer to final concentrations of 0.05 to 2.0 mg/ml. Protein concentrations were determined using the micro Bradford dye assay (Bio-Rad, Hercules, CA). Electron microscopy of protein solutions containing 4 to 10 mg/ml of purified CA protein in 50 mM Tris buffer, pH 8.0, 30 mM NaCl on formvar-carbon grids stained with 2% uranyl acetate revealed large structures similar in morphology to cores isolated from particles assembled in natural infection (Fig. 1; Chrystie and Almeida, 1988; Gelderblom, 1991; Fukui et al., 1993). To prepare dust-free protein solutions for light-scattering measurements, the solutions were filtered through buffer-equilibrated sterile 0.45-μm pore-size membrane filters (Millipore, Bedford, MA) into 17-mm-OD light-scattering cells that were rinsed with distilled acetone to ensure dust-free condition before use.

SLS and DLS

A standard, laboratory-built light scattering spectrometer with an argon ion laser operating at 488 nm was used for the scattering experiments (Chu et al., 1984). The instrument was capable of making both the angular distribution of absolute integrated scattered intensity (SLS) and the time-dependent intensity-intensity time correlation function (DLS) by using photon counting equipment together with a Brookhaven BI-9000 digital correlator. SLS and DLS measurements were performed at scattering angles between 30 and 140°. Results shown below are the average values of triplicate experiments where in every experiment six individual measurements were typically taken at each scattering angle.

For SLS measurements in dilute solution, the relevant equation is known as the Rayleigh-Gans-Debye equation:

$$HC/R_{ex} = 1/M_w(1 + 2A_2M_wC)(1 + q^2R_g^2/3) \qquad (1)$$

where $H\,[= 4\pi^2 n_{Bz}^2(dn/dc)^2/N_A\,\lambda^4]$ is an optical parameter with n_{Bz} being the refractive index of a reference standard solvent (benzene); N_A, Avogadro's constant; λ, the laser wavelength (488 nm); M_w, weight-average molecular weight of the solute; A_2, the second virial coefficient; C, solute concentration; dn/dc, the refractive index increment; $q\,[= 4\pi n \sin(\theta/2)/\lambda]$, the magnitude of the scattering vector with θ, the scattering angle; and R_g, the z-average solute radius of gyration. R_{ex} is the excess Rayleigh ratio of the protein solution and it is equal to $R_{Bz}(I - I_0)/I_{Bz}(n^2/n_{Bz}^2)$, where R_{Bz} is the Rayleigh ratio of benzene; I, I_0, and I_{Bz} are the scattered intensities of the protein solution, the solvent (aqueous buffer) and benzene, respectively; and n is the refractive index of the solvent. In the absence of interference and interactions, the total solute scattered intensity is proportional to the solute concentration and the molecular weight of solute particles. If solute molecules aggregate significantly, the scattered intensity will drastically increase,

$$(I - I_0) \propto C \cdot M_w \qquad (2)$$

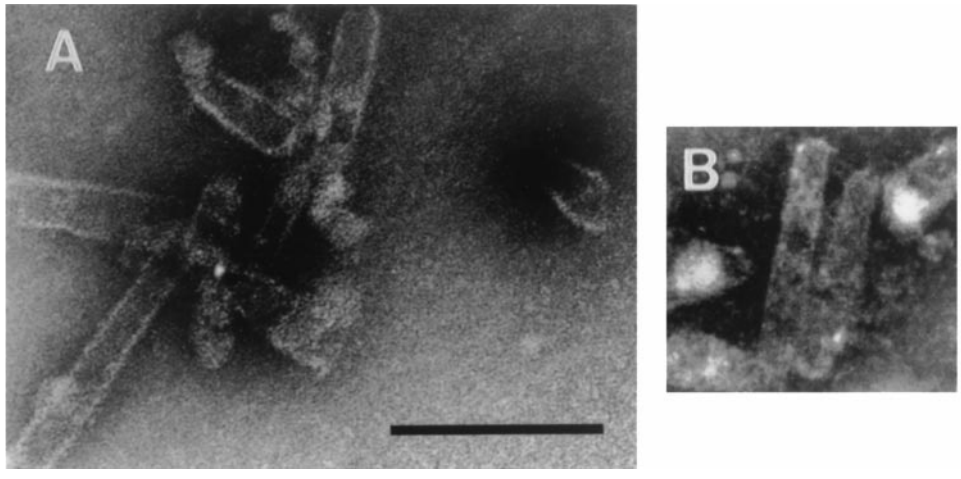

FIGURE 1 Morphology of CA structures detected by negative stain electron microscopy. (*A*) Electron micrograph of negatively stained structures of recombinant HIV CA protein assembled in vitro. (*B*) Electron micrograph of negatively stained cores in HIV viral particles formed during natural infection. Courtesy of I. L. Chrystie. Scale bar, 200 nm

Parameters of particle mass (M_w) and of particle size (R_g) can be determined from Eq. 1.

DLS measures the intensity-intensity time correlation function $G^{(2)}(\Gamma)$ by means of a multi-channel digital correlator (Chu, 1991). This function is defined by Eq. 3:

$$G^{(2)}(\Gamma) = A(1 + b|g^{(1)}(\tau)|^2) \quad (3)$$

where A, b, and $|g^{(1)}(\tau)|$ are, respectively, the background, a coherence factor, and the normalized electric field time correlation function. The field correlation function $|g^{(1)}(\tau)|$ was analyzed by the constrained regularized CONTIN (Provencher, 1976a,b) method, to yield information on the distribution of the characteristic linewidth (Γ) from

$$|g^{(1)}(\tau)| = \int G(\Gamma)e^{-\Gamma\tau}d\Gamma \quad (4)$$

The normalized distribution function of the characteristic linewidth $G(\Gamma)$ so obtained can be used to determine an average apparent translational diffusion coefficient, $D_{app.}$.

$$D_{app.} = \Gamma/q^2 \quad (5)$$

A parameter of particle size, apparent hydrodynamic radius ($R_{h,app.}$) is related to $D_{app.}$ via the Stokes-Einstein equation:

$$R_{h,app.} = k\Gamma/6\pi\eta D_{app.} \quad (6)$$

where k is the Boltzmann constant and η is the viscosity of the solvent at temperature T. The particle-size distribution in solution is obtained from a plot of $\Gamma G(\Gamma)$ versus $R_{h,app.}$, with $\Gamma_i G(\Gamma_i)$ being proportional to the angular-dependent scattered intensity of particle i having an apparent hydrodynamic radius $R_{h,i}$. The relative peak area of each mode represents the contribution to the total scattered intensity due to that kind of particle.

Depolarized DLS measures the rotational diffusion coefficient (Θ) of the macromolecules (Zero and Pecora, 1985). By detecting the depolarized scattered intensity using vertically polarized incident light, I_{VH}, the CONTIN analysis yields a distribution of characteristic linewidth Γ_{VH}, with

$$\Gamma_{VH} = D \cdot q^2 + 6\Theta \quad (7)$$

The magnitude of I_{VH} is related to the molecular anisotropy in solution. By knowing the R_h and Θ values of the particles and assuming that the polydispersity effect is negligible, the particle shape can be estimated by using certain fitting equations (Broersma, 1960; see next section). At least two independent measurements were made for CA protein samples. Similar results were obtained for protein concentrations of 0.05 to 2.0 mg/ml. Analyses at 0.5 mg/ml are described below.

RESULTS

Estimate of the mass of CA protein multimers

The weight-average molecular weight (M_w) and the radius of gyration (R_g) of CA protein multimers were calculated from SLS measurements. For the samples with pH values >6.7, the major contribution to the scattered intensity was made by large assemblages, and the contribution from small oligomers, most likely dimers (Rose et al., 1992; Ehrlich et al., 1992; Momany et al., 1996; Yoo et al., 1997; Berthet-Colominas et al., 1999) was estimated to be negligible, as observed from DLS measurements (described below). At dilute protein concentrations (<10 mg/ml), the interaction between adjacent proteins should be very weak due to the very large protein-protein distance, e.g., the A_2 term in eq. 1 can be neglected; then the M_w and R_g of the assemblages can be calculated without extrapolating the scattered intensity to zero CA concentration. Fig. 2 shows the calculation of M_w of CA multimers from SLS results. At pH 6.8, the M_w of CA multimers assembled in 0.5 mg/ml solutions was ~22.0 MDa. Because the unit quaternary structure of CA is a dimer with a molecular weight of 4.75×10^4 Da, the multimers had an aggregation number of 428 CA dimers. From the slope of the same fitting curve, the R_g of the aggregates was estimated to be ~103 nm by using eq. (1). The M_w decreased with increasing pH value, as shown by the decrease in the total scattered intensity. At pH 7.0, there were only ~240 dimers in each CA multimer, indicating

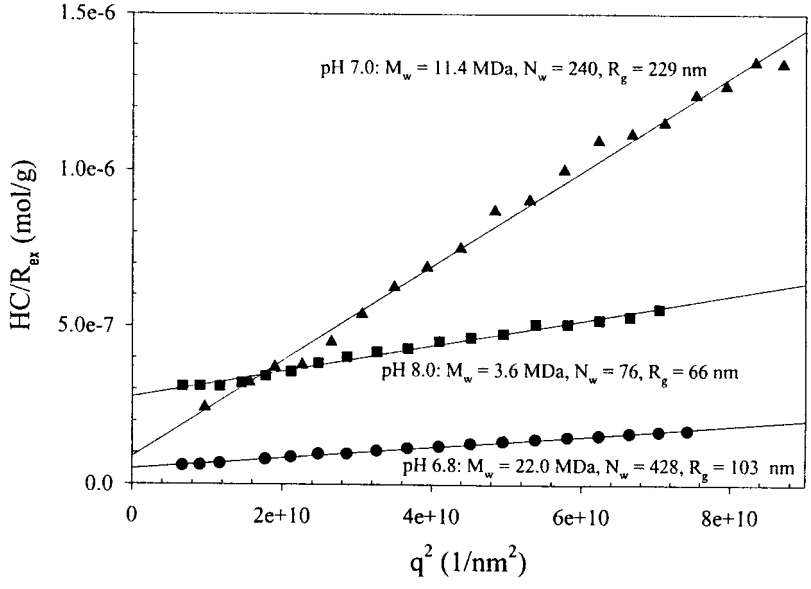

FIGURE 2 SLS measurements of the weight-average molecular weight (M_w) and the radius of gyration (R_g) of CA multimers assembled in 0.5 mg/ml solutions at pH 6.8, 7.0, and 8.0 at room temperature.

that the multimers had been partly dissociated. However, the R_g value of the multimers became even larger (229 nm) than that at pH 6.8 (103 nm), suggesting a pH-sensitive conformational change (discussed below). At pH 8.0, the multimers became even smaller, with only ~76 dimers in each aggregate. The R_g value of the multimer also decreased to only 66 nm. Thus, the association number (N_w) of the CA multimers decreased with increasing pH value.

Consistent with the behavior of other self-associating proteins (Nichol, 1981), N_w of CA multimers showed a strong concentration dependence. A much higher N_w was observed with 2.0 mg/ml CA protein solutions at a fixed pH value (e.g., at pH 7.0, N_w was >600 for 2.0 mg/ml CA, compared with 240 for 0.5 mg/ml CA).

pH-dependent dissociation of CA protein multimers to dimers

The total scattered intensity of 0.5 mg/ml CA protein solution was examined as a function of solution pH using SLS. As shown in Fig. 3, scatter intensity decreased as the pH decreased from pH 7.0 to pH 6.7. Because the protein concentration was the same for all pH conditions, this sharp decrease in the scattered intensity indicated a decrease in the molecular weight of the solute particles. This pH-dependent dissociation of CA multimers occurred mainly within a small pH range of 6.6 and 6.9.

Changes in particle size and size distribution at different pH conditions were examined using DLS (Fig. 4, *A–F*). Particle size was inferred from the hydrodynamic radius (R_h) which is the $R_{h,\,app.}$ value extrapolated to zero scattering angle at finite concentration. At both pH 8.0 and 7.0 (*A* and *B*), two scattering populations were observed, one with an average R_h value of ~100 nm corresponding to the CA multimer and another with a R_h value of 2 to 3 nm corre-

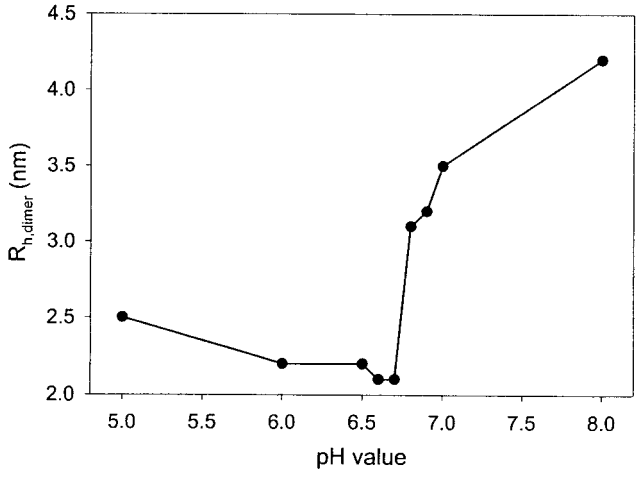

FIGURE 3 Apparent hydrodynamic radius (R_h) of CA dimers at different pH values, measured by DLS at 90° scattering angle.

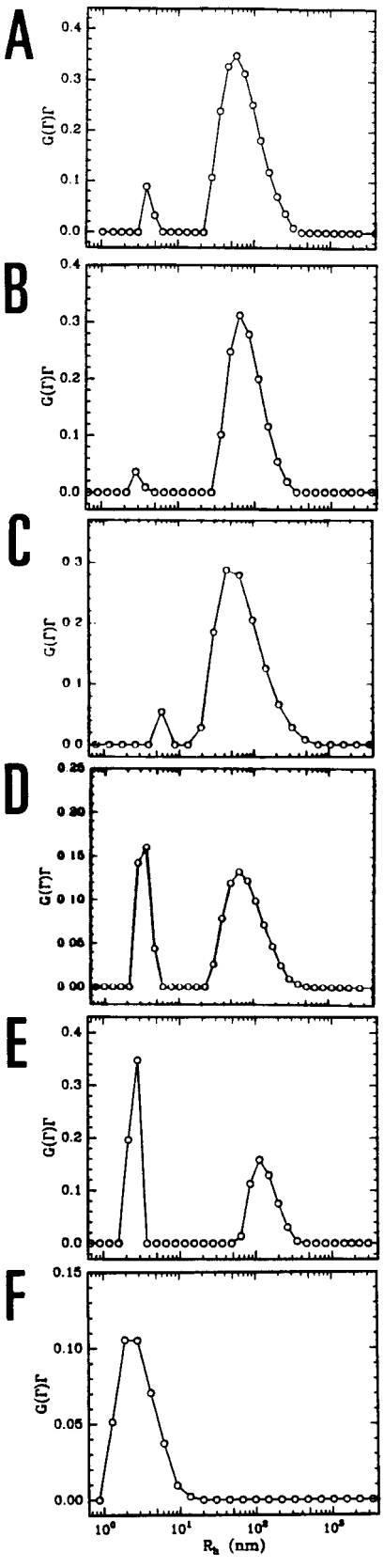

FIGURE 4 CONTIN analysis of DLS measurements on 0.5 mg/ml CA solutions at 90° scattering angle and room temperature: (*A*) pH 8.0; (*B*) pH 7.0; (*C*) pH 6.9; (*D*) pH 6.6; (*E*) pH 6.0; (*F*) pH 5.0.

sponding to CA dimers. Under both pH conditions, the peaks corresponding to multimers were more dominant, suggesting that a larger portion of the CA proteins existed as multimers. However, with decreasing pH value, the relative peak area due to dimers became increasingly larger, indicating that more and more multimers started to dissociate into smaller particles (*D* to *F*). At pH 6.6, the peaks due to multimers and dimers had roughly the same peak areas (*D*). Based on the scattering theory, the large particles can scatter light much more strongly (sixth power to the particle size). Therefore, at pH 6.6, most of the CA protein actually existed as dimers. This inference is consistent with our observation from SLS measurements that the multimer to dimer transition occurred mainly in the pH range of 6.6 to 6.9 (Fig. 3). At a lower pH value (e.g., pH 5.0), only one population, with an R_h value of around 2 to 3 nm, was detected by DLS. Under this condition, all the CA proteins were dimers and no more multimers existed in solution. This condition represents complete dissociation of CA multimers into its component subunits (CA dimers).

pH-dependent conformational change in CA protein dimers

Dimer conformation as a function of pH was examined by plotting the R_h values of dimers *versus* the pH of the protein solution (Fig. 5). As described above, the scattering peaks in DLS measurements at the position between 1 and 10 nm can be attributed to the CA protein dimers. The R_h values of dimers varied between 2.1 and 4.2 nm, with the minimum value (2.1 nm) appearing at around pH 6.6. This change in the R_h value of the CA dimers indicated that the conformation was more extended at higher pH. A similar phenomenon has been studied in long-chain polymers, often referred to as the coil to globule transition where the coil state refers to an extended chain conformation and the globule state denotes a compact conformation (Wu and Zhou, 1995). Additionally, the solubility of a protein in an aqueous solution should reach a minimum value at the isoelectric point, when positive and negative charges are equivalent. For the CA protein, the isoelectric point is pH 6.7. Therefore, it is reasonable for the CA protein to have the lowest R_h around that pH value.

pH-dependent conformational change in CA protein multimers

The shape of the CA multimers was assessed from the ratio of R_g (from SLS) and R_h (from DLS). For a solid homogeneous sphere, R_g/R_h is equal to 0.773. This ratio increases when the conformation becomes more anisotropic (i.e., extended). A long rod-like shape is usually indicated by a R_g/R_h ratio of > 2. For CA protein multimers at pH 6.8, 7.0, and 8.0, $R_h = 137$, 125, and 62 nm, respectively. Taking R_g from the data in Fig. 2, we obtain $R_g/R_h = 0.75$, 1.83, and 1.07, respectively. These values suggest that at pH 6.8, CA protein multimers are essentially spherical. At pH 7.0, anisotropy in shape occurs which decreases with a further increase in the pH value.

It should be noted that when using R_g/R_h ratio to describe the particle conformation, the polydispersity index should also be considered. In the current case, the average ($\mu_2/\bar{\Gamma}^2$) value (with $\mu_2 = \int(\Gamma - \bar{\Gamma})^2 G(\Gamma) d\Gamma$ and $\bar{\Gamma} = \int \Gamma G(\Gamma) d\Gamma$) is around 0.04 for the CA multimers, corresponding to a polydispersity index of ~1.16. This value is sufficiently small to render the above analysis meaningful.

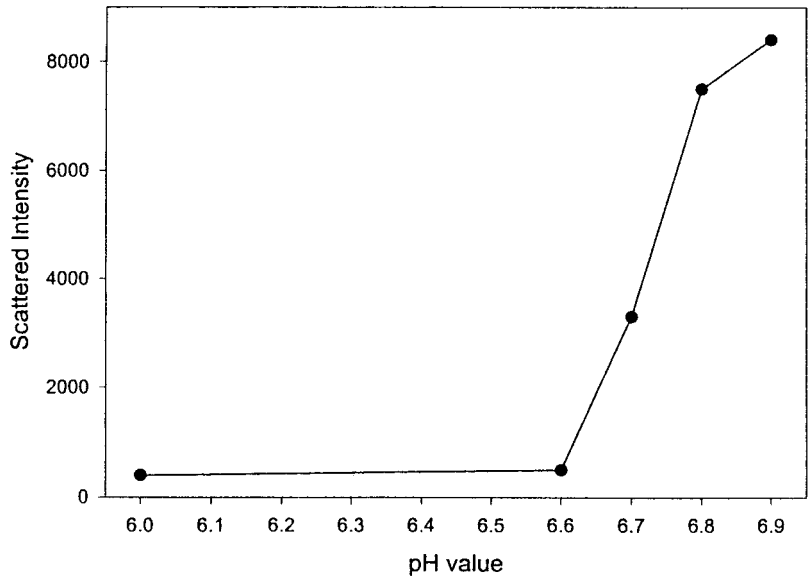

FIGURE 5 pH-dependence of total scattered intensity of a 0.5 mg/ml CA protein solution, measured at 90° scattering angle.

Dimensions of the rod-like CA multimer

A detailed SLS, DLS and depolarized DLS study of the conformation of the multimer in the 0.5 mg/ml, pH 7.0 solution was carried out to obtain values of length and diameter of the anisotropic multimers in this solution. Because the multimer is non-spherical, depolarization in the scattered intensity can be expected. Depolarized DLS measurements showed a single peak with an average apparent Γ of 1.54×10^3 s^{-1}. This value should be attributable to the multimer, and not the dimer, because, by virtue of their smaller size, dimers are expected to rotate too fast to allow Θ measurement by our current instrument.

The conformation of the multimers can be estimated by fitting the translational and rotational diffusion coefficients, with certain well-established methods. The widely accepted Broersma's relations (Broersma, 1960) for long rods ($L/d > 4$, with L and d being the length and the diameter, respectively, of the cylinders) is a reasonable model for highly-anisotropic particles.

$$D = \frac{kT}{3\pi\eta_0 L}\left[6 - \frac{1}{2}(\gamma_{\parallel} + \gamma_{\perp})\right] \tag{8}$$

$$\Theta = \frac{3kT}{\pi\eta_0 L^3}(\delta - \zeta) \tag{9}$$

where

$$\delta = \ln(2L/d)$$

$$\gamma_{\parallel} = 1.27 - 7.4(1/\delta - 0.34)^2$$

$$\gamma_{\perp} = 0.19 - 4.2(1/\delta - 0.39)^2$$

$$\zeta = 1.45 - 7.5(1/\delta - 0.27)^2$$

The diffusion coefficients best fit a rod with length $L = 770$ nm and diameter $d = 45$ nm. These values are in good agreement with previous results obtained using EM ($d = 30$ to 80 nm, $L = 100$ to > 800 nm) (Ehrlich et al., 1992; Gross et al., 1997; von Schwedler et al., 1998; Gross et al., 2000). This result is reasonable because a corresponding cylindrical particle should have a R_g value of 223 nm, which is very close to the measured R_g value (229 nm) by SLS (Fig. 2). Also, a cylinder with that size should have a theoretical hydrodynamic radius ($R_{h,0}$) of ~140 nm, which is similar to the empirical value of 125 nm (Fig. 5). The small discrepancy can be attributed to the fact that the measured value is the effective R_h at finite concentrations. At present, we cannot distinguish the difference between a long rod and a prolate ellipsoid because their values become similar when the length becomes much greater than the radius. We also tried to fit the data to an oblate ellipsoid using the Perrin relation (Koenig, 1975), however, no reasonable fitting result could be obtained, suggesting that the CA multimers did not have an oblate ellipsoidal shape.

The weight percentage that measures the amount of multimers in the pH 7 solution, was estimated by extrapolating the total scattered intensities of the scattering entities to zero scattering angle. The dimers are too small to have any angular dependence on scattered intensity. The scattering curve of the multimers is dependent on their conformation. An expression for the form factor (P) of a rigid-rod particle with length L is given below:

$$P(qL) = \frac{2}{qL}\cdot\int_0^{qL}\left(\frac{\sin x}{x}\right)dx - \left[\frac{2}{qL}\cdot\sin\left(\frac{qL}{2}\right)\right]^2 \tag{10}$$

For CA multimers at pH 7.0 ($L = 770$ nm), its scattered intensity at 45° scattering angle ($q = 0.013$ nm^{-1}) is equivalent to ~¼ of the scattered intensity at 0° scattering angle. At the same time, CONTIN analysis revealed that at 45° scattering angle, the scattered intensity due to multimers was ~150 times stronger than that of dimers. Considering that each multimer contains, on average, ~240 dimers, we have:

$$\frac{240M_w\cdot\alpha}{M_w\cdot(0.5-\alpha)} = 150\times 4 = 600 \tag{11}$$

with α being the weight concentration of multimers. Calculations indicate that a significant amount (>70%) of CA molecules existed as multimers in the pH 7.0 solution.

DISCUSSION

Our study revealed that pH induced a transition in CA dimer conformation and in CA multimer morphology. Gross differences in conformation were assessed from the R_h value calculated for the dimer present in each CA protein solution. R_h of dimers present in the pH 6.6 protein solution had a calculated value of 2.1 nm whereas those present in the pH 7.0 protein solution had a calculated value of 3.7 nm. We interpret this rise in R_h value as a shift to a relatively less compact dimer conformation as pH was increased. The morphology of CA multimers in these solutions was characterized from the ratio of R_g over R_h. At pH 6.8, R_g/R_h was equal to 0.75, indicating a spherical morphology. At pH 7.0, the multimer R_g/R_h ratio increased to 1.83 consistent with a rod-like morphology. The intrinsic ability of CA multimers to assume a rod-like morphology has been shown previously in EM studies of structures formed by recombinant CA protein (Ehrlich et al., 1992; Gross et al., 1997, 2000; von Schwedler et al., 1998). However, that the CA multimer is also capable of assuming a spherical morphology is documented for the first time here. Rules governing subunit packing deciphered from capsid structures of simpler, unenveloped, RNA plant viruses indicate that a rod-like morphology is obtainable with packing of subunits in a hexameric pattern, whereas the spherical morphology requires that some subunits be packed in a pentameric pattern to achieve

the necessary curvature (Caspar and Klug, 1962; Phelps et al., 2000). Both packing patterns were shown to participate in the in vitro assembly of conical models of the HIV-1 core (Ganser et al., 1999). Hence, the change in CA multimer morphology from rod-like to spherical may reflect changes in conformation and contacts in a subset of CA proteins in the multimer.

We also observed instability of CA multimers to mildly acidic conditions. As the pH of the solution was lowered, multimers progressively diminished with concomitant increase in dimers. The multimer to dimer transition was clearly evident at pH 6.6, and was essentially complete at pH 6.0. Given the spherical morphology of the CA multimer at pH 6.8, the absence of dissociation products of intermediate size representing either hexameric or pentameric grouping of dimers is noteworthy. Evidently, such intermediates, if they exist, were not stable, sugggesting that putative dimer-dimer contacts were labilized. Relative scattering intensities from pH 6, pH 7, and pH 8 CA protein solutions remained the same as NaCl was incrementally added to a 2.0 M final concentration (data not shown) indicating minimal influence of salt on the pH-dependence of the transition. The finding that the multimer is unstable in mildly acidic conditions is in sharp contrast to the stability exhibited by the monomer and the dimer. Misselwitz et al. (1995) reported that HIV-1 CA protein, as monitored by circular dichroism and fluorescence spectroscopy, was stable to mildly acidic conditions, showing signs of spectral changes only upon reaching a pH of 3.6. Rose et al. (1992) reported that monomer-dimer equilibria were, likewise, unperturbed between pH 8 and pH 5 yielding relatively invariant dissociation constants (i.e., 3.9×10^{-5} M and 1.3×10^{-5} M, respectively) with an increase in dissociation observable only at pH 4 (i.e., Kd of 5.4×10^{-6} M). Our observation of a transition from multimer to dimer at pH 6.6 suggests that, in contrast, dimer-dimer interfaces are easily perturbed.

Because pH was the only variable introduced in these experiments, the likely initiating molecular event for the transitions observed is protonation of one or several titratable CA residues in the pH range. As shown above, multimer to dimer transition, as well as multimer morphology and dimer conformation transitions, occurred between pH 6.6 and pH 6.9. This suggests histidine as a possible candidate for the titratable residue, the protonation of which serves as switch for these transitions. This function has been attributed to histidine in disassembly of foot-and-mouth-disease virus capsids and subsequently corroborated by both computational and mutational analyses (Yang and Honig, 1993; Ellard et al., 1999). Detection of dimers as the only product of CA multimer dissociation suggests a model for the spherical multimer where histidine residues exert significant influence on interfaces that hold dimer subunits together but not on the dimerization interface itself. In the HIV-1 CA polypeptide, there are a total of five histidine residues, three of which are highly conserved among the different HIV clades (His12, His62, and His84). Models of the CA protein structure (Berthet-Colominas et al., 1999; Gamble et al., 1996, 1997; Gitti et al., 1996; Momany et al., 1996) show all five His residues to be surface localized and part of non-helix, non-β structures. Four are in the N-terminal domain (His12, His62, His84, and His87) and one in the C-terminal domain (His226). His226 in the C-terminal domain is predicted to be positioned away from the CA protein dimerization interface (Gamble et al., 1997) and should have minimal influence on dimer stability. His12 and His62 are located on a face that serves as an interface in a symmetrical side-to-side association of two N-terminal domains (Gamble et al., 1996). Protonation of the imidazole side chain in one or both His residues could result in electrostatic repulsion that may weaken dimer-dimer association through this interface. His84 and His 87 are located on a non-interface surface in structures showing associated N-terminal domains (Gamble et al., 1996; Momany et al., 1994). However, protonation of either one could initiate changes that have distal effects.

The morphological transitions induced by pH and possible roles of the novel spherical multimer are suggested schematically in Fig. 6. Whether or not pH serves as a cue for capsid disassembly during HIV virus entry, it is known that HIV particles utilize both receptor-mediated and endocytic entry modes for internalization during natural infection (Grewe et al., 1990; Marechal et al., 1998; Fackler and Peterlin, 2000; Schaeffer et al., 2001). It has been maintained that vesicular internalization does not participate in the infectious pathway because productive replication was found to correlate with internalization in the cytosol rather than in endocytic vesicles (Marechal et al., 1998). Moreover, Nef, a viral accessory protein that facilitates viral replication, enhances internalization by receptor-mediated plasma membrane fusion (Schaeffer et al., 2001). However, several studies document productive replication of HIV particles internalized by endocytosis (Fackler and Peterlin, 2000; Aiken, 1997; Marechal et al., 1998). Thus, low pH, in itself, does not lead to a dead end route for HIV. Low pH has been implicated in cell entry and RNA release by picornaviruses (Phelps et al., 2000). The capsids of foot-and-mouth-disease virus and mengovirus, which both enter via the endocytic pathway during natural infection, are dissociated at low pH into the unique pentameric units that serve as assembly protomers for these spherical viruses. The capsids of rhinovirus and poliovirus, which both enter via receptor-mediated pathways during natural infection, are structurally altered by low pH resulting in the same conformational changes induced by receptor binding. Perhaps, for HIV, the replication competence of the entry pathway is determined by the CA disassembly mode. This could be the case if environmental cues associated with receptor-mediated and endocytic entry elicit different conformational changes in the CA protein that, in turn, result in different disassembly modes leading, for example, to dimeric disas-

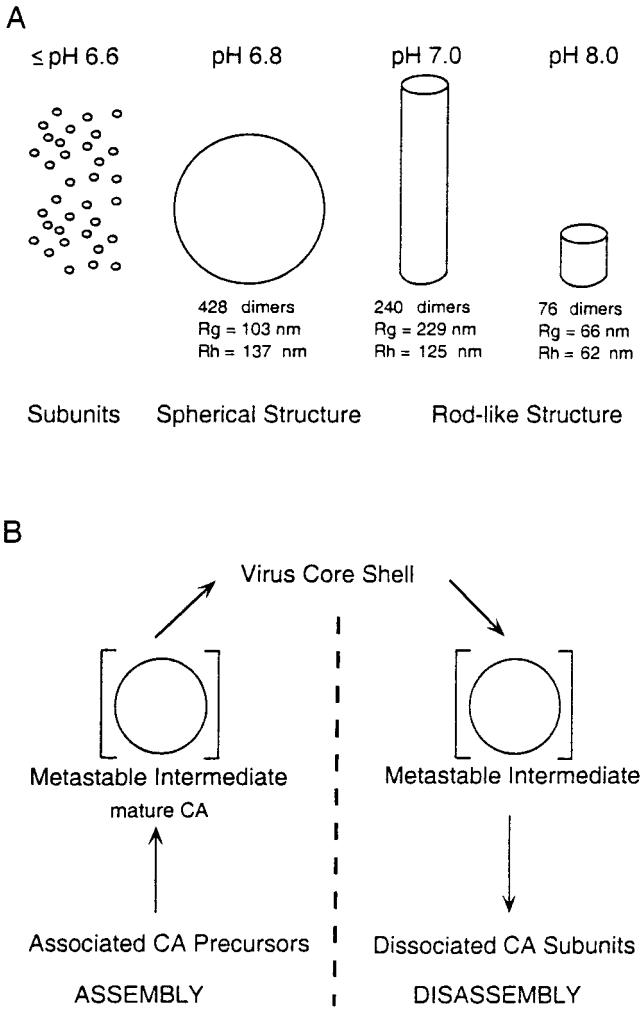

FIGURE 6 (*A*) Range of CA protein response to an environmental cue (pH) detected by DLS. (*B*) Possible roles of the novel spherical CA multimer in virus replication.

sembly products in one case versus pentameric products in the other.

This study was supported by grant DMR9612386 from the National Science Foundation (to B.C.), and National Institutes of Health grants GM48294 (to C.C.) and GM58271 (to S.S. and C.C.).

REFERENCES

Aiken, C. 1997. Pseudotyping human immunodeficiency virus type 1 (HIV-1) by the glycoprotein vesicular stomatitis virus targets HIV-1 entry to an endocytic pathway and suppresses both the requirement for Nef and the sensitivity to cyclosporin A. *J. Virol.* 71:5871–5877.

Berthet-Colominas, C., S. Monaco, A. Novelli, G. Sibai, F. Mallet, and S. Cusack. 1999. Head-to-tail dimers and interdomain flexibility revealed by the crystal structure of HIV-1 capsid protein (p24) complexed with a monoclonal antibody Fab. *EMBO J.* 18:1124–1136.

Broersma, S. 1960. Translational diffusion constant of a random coil. *J. Chem. Phys.* 32:1626–1632.

Caspar, D. L. D., and A. Klug. 1962. Physical principles in the construction of regular viruses. *Cold Spring Harbor Symp. Quant. Biol.* 27:1–24.

Chrystie, I. L., and J. D. Almeida. 1988. The morphology of human immunodeficiency virus (HIV) by negative staining. *J. Med. Virol.* 25:281–288.

Chu, B. 1991. Laser Light Scattering. Academic Press, Inc., New York.

Chu, B., M. Onclin, and J. R. Ford. 1984. Laser-light scattering characterization of polyethylene in 1,2,4-trichlorobenzene. *J. Phys. Chem.* 88:6566–6575.

Ehrlich, L. S., B. E. Agresta, and C. A. Carter. 1992. Assembly of recombinant human immunodeficiency virus type 1 capsid protein in vitro. *J. Virol.* 66:4874–4883.

Ehrlich, L. S., H.-G. Kräusslich, E. Wimmer, and C. Carter. 1990. Expression in *Escherichia coli* and purification of human immunodeficiency virus type 1 capsid protein (p24). *AIDS Res. Hum. Retrovir.* 6:1169–1175.

Ellard, F. M., J. Drew, W. E. Blakemore, S. I. Stuart, and A. M. Q. King. 1999. Evidence for the role of His-142 of protein 1C in the acid-induced disassembly of foot-and-mouth disease virus capsids. *J. Gen. Virol.* 80:1911–1918.

Fackler, O. T., and B. M. Peterlin. 2000. Endocytic entry of HIV-1. *Curr Biol* 10:1005–1008.

Fukui, T., S. Imura, T. Goto, T., and M. Nakai. 1993. Inner architecture of human immunodeficiency and simian immunodeficiency virus. *Microsc. Res. Tech.* 25:335–340.

Gamble, T. R., F. F. Vajdos, S. Yoo, D. K. Worthylake, M. Houseweart, W. I. Sundquist, and C. P. Hill. 1996. Crystal structure of human cyclophilin A bound to the amino terminal domain of HIV-1 capsid. *Cell.* 87:1285–1294.

Gamble, T. R., S. Yoo, F. F. Vajdos, U. K. von Schwedler, D. K. Worthylake, H. Wang, J. P. McCutcheon, W. I. Sundquist, and C. P. Hill. 1997. Structure of the carboxyl-terminal dimerization domain of the HIV-1 capsid protein. *Science.* 278:849–853.

Ganser, B. K., S. Li, V. Y. Klishko, J. T. Finch, and W. I. Sundquist. 1999. Assembly and analysis of conical models for the HIV-1 core. *Science.* 283:80–83.

Gelderblom, H. R. 1991. Assembly and morphology of HIV: potential effect of structure on viral function. *AIDS.* 5:617–638.

Gitti, R. K., B. M. Lee, J. Walker, M. F. Summers, S. Yoo, and W. I. Sundquist. 1996. Structure of the amino-terminal core domain of the HIV-1 capsid protein. *Science.* 273:231–235.

Grewe, C., A. Beck, and H. R. Gelderblom. 1990. HIV: early virus-cell interactions. *J. Acquir. Immune Defic. Syndr.* 3:965–974.

Gross, I., H. Hohenberg, and H.-G. Kräusslich. 1997. In vitro assembly properties of purified bacterially expressed capsid proteins of human immunodeficiency virus. *Eur. J. Biochem.* 249:592–600.

Gross, I., H. Hohenberg, T. Wilk, K. Wiegers, M. Grattinger, B. Muller, S. Fuller, and H.-G. Kräusslich. 2000. A conformational switch controlling HIV-1 morphogenesis. *EMBO J.* 19:103–113.

Koenig, S. H. 1975. Brownian motion of an ellipsoid. A correction to Perrin's results. *Biopolymers.* 14:2421–2423.

Marechal, V., F. Clavel, J. M. Heard, and O. Schwartz. 1998. Cytosolic Gag p24 as an index of productive entry of human immunodeficiency virus type 1. *J. Virol.* 72:2208–2212.

Marsh, M. 1984. The entry of enveloped viruses into cells by endocytosis. *Biochem. J.* 218:1–10.

Misselwitz, R., G. Hausdorf, K. Welfle, W. E. Höhne, and H. Welfe. 1995. Conformation and stability of recombinant HIV-1 capsid protein p24 (rp24). *Biochim. Biophys. Acta.* 1250:9–18.

Momany, C., L. C. Kovari, A. Prongay, W. Keller, R. K. Gitti, B. M. Lee, A. E. Gorbalenya, L. Tong, J. McClure, L. S. Ehrlich, M. F. Summers, C. Carter, and M. G. Rossmann. 1996. Crystal structure of dimeric HIV-1 capsid protein. *Nature Struct. Biol.* 3:763–770.

Nichol, L. W. 1981. Protein Interaction Patterns. *In* Protein-Protein Interactions. Frieden, C. and L. W. Nichol, editors. John Wiley and Sons, New York.2–26.

Phelps, D. K., B. Speelman, and C. B. Post. 2000. Theoretical studies on viral capsid proteins. *Curr. Opin. Struct. Biol.* 10:170–173.

Provencher, S. W. 1976a. Fourier method for analysis of exponential decay curves. *Biophys. J.* 16:27–41.

Provencher, S. W. 1976b. Eigenfunction expansion method for analysis of exponential decay curves. *J. Chem. Phys.* 64:2773–2777.

Rosé, S., P. Hensley, D. J. O'Shannessy, J. Culp, C. Debouck, and I. Chaiken. 1992. Characterization of HIV-1 p24 self-association using analytical affinity chromatography. *Proteins.* 13:112–119.

Schaeffer, E., R. Geleziunas, and W. C. Greene. 2001. Human immunodeficiency virus type 1 nef functions at the level of virus entry by enhancing cytoplasmic delivery of virions. *J. Virol.* 75:2993–3000.

von Schwedler, U. K., T. L. Stemmler, V. Y. Klishko, S. Li, K. H. Albertine, D. R. Davis, and W. I. Sundquist. 1998. Proteolytic refolding of the HIV-1 capsid protein amino terminus facilitates viral core assembly. *EMBO J.* 17:1555–1568.

Welker, R., H. Hohenberg, U. Tessmer, C. Huckhagel, and H.-G. Kräusslich. 2000. Biochemical and structural analysis of isolated mature cores of human immunodeficiency virus type 1. *J. Virol.* 74:1168–1177.

Wu, C., and S. Zhou. 1995. Laser-light scattering study of the phase-transition of poly(N-isopropylacrylamide) in water. 1. Single chain. *Macromolecules.* 28:8381–8387.

Yang, A., and B. Honig. 1993. On the pH dependence of protein stability. *J. Mol. Biol.* 231:459–474.

Yoo, S., D G. Myszka, C.-y. Yeh, M. McMurray, C. P. Hill, and W. I. Sundquist. 1997. Molecular recognition in the HIV-1 capsid/cyclophilin A complex. *J. Mol. Biol.* 269:780–795.

Zero, K., and R. Pecora. 1985. Dynamic Depolarized Light Scattering. *In* Dynamic Light Scattering: Applications of Photon Correlation Spectroscopy. R. Pecora, editor. Plenum Press, New York.